J Biol Inorg Chem (2006) 11: 153–167
DOI 10.1007/s00775-005-0060-y

ORIGINAL ARTICLE

**Giampiero De Sanctis · Giovanni Francesco Fasciglione
Stefano Marini · Federica Sinibaldi · Roberto Santucci
Enrico Monzani · Corrado Dallacosta · Luigi Casella
Massimo Coletta**

pH-dependent redox and CO binding properties of chelated protoheme-L-histidine and protoheme-glycyl-L-histidine complexes

Received: 20 June 2005 / Accepted: 4 November 2005 / Published online: 10 December 2005

Abstract The pH dependence of redox properties, spectroscopic features and CO binding kinetics for the chelated protohemin-6(7)-L-histidine methyl ester (heme-H) and the chelated protohemin-6(7)-glycyl-L-histidine methyl ester (heme-GH) systems has been investigated between pH 2.0 and 12.0. The two heme systems appear to be modulated by four protonating groups, tentatively identified as coordinated H_2O, one of heme's propionates, Nε of the coordinating imidazole, and the carboxylate of the histidine residue upon hydrolysis of the methyl ester group (in acid medium). The pK_a values are different for the two hemes, thus reflecting structural differences. In particular, the different strain at the Fe–N_ε bond, related to the different length of the coordinating arm, results in a dramatic alteration of the bond strength, which is much smaller in heme-H than in heme-GH. It leads to a variation in the variation of the p*Ka* for the protonation of the N_ε of the axial imidazole as well as in the proton-linked behavior of the other protonating groups, envisaging a cross-talk communication mechanism among different groups of the heme, which can be operative and relevant also in the presence of the protein matrix.

Keywords Heme model systems · pH dependence · Redox properties · Absorption spectra · CO binding kinetics

Electronic Supplementary Material Supplementary material is available for this article at http://dx.doi.org/10.1007/s00775-005-0060-y and is accessible for authorized users.

G. De Sanctis
Department of Molecular, Cellular and Animal Biology,
University of Camerino, Via F. Camerini 2, 62032 Camerino, Italy

G. F. Fasciglione · S. Marini · F. Sinibaldi
R. Santucci · M. Coletta (✉)
Department of Experimental Medicine and Biochemical Sciences,
University of Roma—Tor Vergata, Via Montpellier 1,
00133 Roma, Italy
E-mail: coletta@seneca.uniroma2.it
Tel.: +39-6-72596365
Fax: +39-6-72596353

E. Monzani · C. Dallacosta · L. Casella
Department of General Chemistry, University of Pavia,
Via Taramelli 12, 27100 Pavia, Italy

Introduction

Heme proteins represent a family of proteins and enzymes displaying a large variety of activities promoted by their prosthetic group. A better understanding of their properties may be achieved by the synthesis of iron–porphyrin model systems and by the characterization of the factors affecting the electronic, spectroscopic and structural properties of these smaller molecules. Many heme proteins (including myoglobin, hemoglobin, guanylate cyclase and several peroxidases) possess the prosthetic group protoheme IX, which is usually axially coordinated by a single histidine residue on the side opposite that involved in binding of exogenous ligands or assigned to the catalytic activity [1]. The strength of the axial imidazole coordination contributes to the complex pattern of factors controlling the activity of these proteins [2, 3]. The axial binding strength can generally be modulated through three main mechanisms: (1) the hydrogen-bonding interaction between the imidazole and a nearby carboxylate group [4]; (2) a change in the orientation of the imidazole plane [5, 6]; and (3) the introduction of a conformational strain as a consequence of the binding of the proximal residue, producing some tilting of the imidazole group [7].

With the aim of studying these effects, several chelated iron–porphyrin model systems have been synthesized, containing an appended imidazole residue which can intramolecularly bind to the iron center [8–19]. A different approach involves the use of heme–peptide complexes (called microperoxidases) obtained from the

proteolysis of horse heart cytochrome *c* [20, 21]. However, while bearing the advantages of good water solubility and reduced tendency to aggregate, which are helpful for the comparison with the proteins, microperoxidases suffer the problem of containing a different type of heme (heme *c*) in their structure. Furthermore, the C-terminal peptide sequence containing the iron–imidazole axial ligand prevents the possibility of introducing structural or conformational limitations on the histidine coordination.

For these reasons, covalently modified protohemin or deuterohemin complexes, obtained by linking amino acids or peptides to the propionate side chains of the porphyrin, represent the most suitable systems to investigate stereochemical and conformational effects introduced by the chelated axial ligand and, in some cases, also the modulation of the iron–axial ligand interaction [8–12, 18, 19]. Complexes of this type have generally been used to investigate the ligand binding properties of the iron center, as peroxidase mimics as well as modified cofactors for reconstituted proteins [22–24]. To show the effect of strain in the axial ligand on the binding and catalytic properties of the iron center, a group of deuterohemins containing a histidine residue bound in a side arm with variable length were previously used [18]. As a matter of fact, the importance of strain on the proximal axial bond of the heme has been demonstrated in several papers, clearly indicating that it plays a relevant role not only in the reactivity of the heme [2, 3, 25], but also in the modulation of cooperativity in hemoglobin [26, 27]. In this work we have investigated the pH dependence of the spectral, redox and the CO binding properties of protohemin-6(7)-L-histidine methyl ester (heme-H) and protohemin-6(7)- glycyl-L-histidine methyl ester (heme-GH), where a L-histidine methyl ester or a glycyl-L-histidine methyl ester residue is bound to one of the propionate chains, respectively (Scheme 1). On the basis of the properties of the corresponding deuterohemin derivatives [18], it can be assumed that in heme-H the histidine coordination is more strained than in heme-GH, allowing us to investigate in greater detail the proximal strain effect on heme properties.

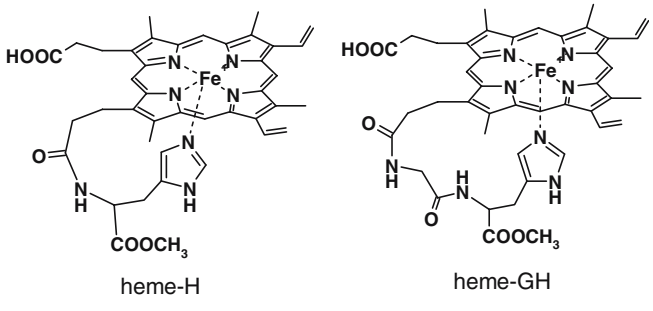

Scheme 1 Structures of protohemin-6(7)-L-histidine methyl ester (*heme-H*) and protohemin-6(7)-glycyl-L-histidine methyl ester (*heme-GH*)

Experimental

Sample preparation

Glycyl-L-histidine methyl ester dihydrochloride was prepared by esterification with methanol of glycyl-L-histidine dihydrochloride (Sigma) following a literature method [19].

Heme-GH and heme-H were obtained by condensation of glycyl-L-histidine methyl ester or L-histidine methyl ester (Sigma), respectively, to one of the propionate arms of hemin, following a procedure similar to that reported recently for heme-GH [28]. A solution of protohemin chloride (300 mg, 0.46 mmol), 1-hydroxybenzotriazole (310 mg, 2.3 mmol), *O*-(benzotriazol-1-yl)-*N*,*N*,*N*′,*N*′-tetramethyluronium hexafluorophosphate (175 mg, 0.46 mmol) and triethylamine (255 µl, 1.8 mmol) in freshly distilled dimethylformamide (10 ml) was stirred for 15 min at room temperature. Then, glycyl-L-histidine methyl ester dihydro chloride or L-histidine methyl ester dihydrochloride (0.46 mmol) was added, and the mixture was allowed to react overnight under stirring at room temperature. The dropwise addition of a small amount of water (about 5 ml) caused precipitation of the hemin derivative. The mixture was centrifuged and the solid residue collected. This residue was carefully dried under vacuum and subsequently treated several times with diethyl ether and then filtered to remove the remaining traces of organic reagents. The residue was finally dried under vacuum, adsorbed on inert sand and loaded onto a silica gel column (60×4 cm^2). Chromatographic separation of the modified hemins from unreacted hemin was carried out using a mixture of *n*-butanol–water–acetic acid 4:1:1 (v/v/v) as the eluent. Upon removal of the solvent under vacuum, the samples were further purified by high-performance liquid chromatography (HPLC) using a JASCO MD-1510 instrument with diode array detection and a Supelco C_{18} reversed-phase column (10×250 mm^2). HPLC runs were carried out using a mixture of distilled water–acetonitrile 65:35 (v/v) containing 0.1% trifluoroacetic acid as the eluent; the flow rate was 5 ml/min. Spectrophotometric detection of the eluate was performed in the range 200–600 nm. The retention times of heme-H and heme-GH were 10.0 and 17.6 min, respectively. The purified products exhibit electrospray ionization mass spectrometry spectra (LCQ-DECA ion trap instrument, Thermo-Finnigan) with parent peaks at m/z 767.4 $[M]^+$, for heme-H, and m/z 823.3 $[M\text{-}1]^+$, for heme-GH, in agreement with formulation.

Cyclic voltammetry

Direct current cyclic voltammetry was carried out at 20 °C employing, as a working electrode, a pyrolytic graphite electrode (3-mm diameter, Amel) modified as previously described [29]. Briefly, the heme samples in

phosphate buffer, pH 7.0, were mixed with a tributylmethyl phosphonium chloride resin previously solubilized in dimethyl sulfoxide (DMSO), to form a final 30% (v/v) DMSO–aqueous solution; alternatively, the hemes were dissolved in pure DMSO without an aqueous solution in order to distinguish the DMSO effect from that of the aqueous solution. The electrode modification was achieved by drying 5 µl of the solution on the electrode surface, at 5 °C. Cyclic voltammograms were run at 20 °C in the potential range +200 to −600 mV (vs. the standard calomel electrode), at scan rates of 0.05–1.00 V/s. Measurements were carried out in 0.05 M acetate (pH < 5.5), 0.05 M phosphate (pH range, 5.5–8.0) and 0.05 M carbonate (pH > 9.0) buffers, all containing 0.1 M $KClO_4$ as the supporting electrolyte.

The redox potentials determined at various pH values were analyzed according to the following equation:

$$E_{obs} = E_0 \frac{\sum_{i=0}^{n} \prod_{r=0}^{i} {}^{red}K_{ar}[H^+]}{\sum_{i=0}^{n} \prod_{r=0}^{i} {}^{ox}K_{ar}[H^+]}, \quad (1)$$

where E_{obs} is the redox potential determined at a given pH value, E_0 is the redox potential of the form present at the limit of high pH, ${}^{red}K_a$ and ${}^{ox}K_a$ are the proton association constants of an ionizing functional group in the reduced and oxidized iron porphyrins, respectively (such as $K_a = 10^{pK_a}$, where n is the total number of such redox-linked functionalities. In Eq. 1 we define ${}^{red/ox}K_{a0} \times [H^+] = 1$.

Spectroscopic and kinetics studies

Ferric heme solutions in 30% DMSO were diluted with buffer containing 30% DMSO at the appropriate pH value and the heme iron was reduced in a gas-tight syringe under anaerobic condition by adding sodium dithionite (to a final concentration of 1 mg/ml); alternatively, the heme complexes were dissolved in pure DMSO without an aqueous solvent in order to distinguish the effect of DMSO from that of H_2O. Absorption spectra were obtained employing a JASCO V-530 spectrophotometer; the samples were very stable in sodium dithionite as long as they were kept in anaerobic conditions in a tonometer provided with a 1-cm-pathlength cuvette at the bottom. Fast kinetics was obtained, employing a stopped-flow instrument (Applied Photophysics, Salisbury, UK) with 1-ms dead time. Samples for kinetics experiments were prepared by adding sodium dithionite (to a final concentration of 1 mg/ml) to the ferric heme solution in a very low ionic strength buffer at pH 7.0 under anaerobic conditions in an air-tight syringe. The pH dependence of CO binding kinetics was determined by mixing the reduced heme sample in a very low ionic strength buffer at pH 7.0 with a high ionic strength buffer ($I = 0.15$ after mixing) at the desired pH and CO concentration. Desired CO concentrations were obtained by appropriate dilution of a stock CO-saturated H_2O solution (1×10^{-3} M CO at 20 °C under 1 atm of gaseous CO). The actual pH at which the reaction occurred was measured after the mixing.

Solvent conditions

The DMSO–H_2O ratio was chosen in order to abolish the aggregation probability; thus, while in pure aqueous solutions the voltammetry signal was vanishingly small, clearly indicating the presence of aggregates, the addition of DMSO led to the appearance of a progressively increasing signal, indicating the displacement of the equilibrium in favor of the monomeric species (Fig. 1a). The increase in signal intensity was maximized at approximately 20% DMSO–H_2O ratio and essentially no further change of signal quality was observed between 30% DMSO–H_2O and 100% DMSO, clearly indicating that under our experimental conditions all molecules were in the monomeric form.

A similar effect is observed for the kinetics of CO binding, which shows a markedly biphasic behavior in pure aqueous solutions, with a fast phase followed by a very slow one. Addition of DMSO brought about the progressive disappearance of the slow phase, with a concomitant increase of the amplitude of the fast phase, leaving the rate constant unaffected (Fig. 1b). The slow phase disappears for a ratio of 20% DMSO–H_2O, as observed for the DMSO dependence of the intensity of the voltammetric signals.

Data analysis

Absorbance spectroscopic data as a function of pH were analyzed at different wavelengths according to the following equation:

$$OD_{obs} = OD_0 + \sum_{i=0}^{n} DOD_i \frac{\prod_{r=0}^{i} K_{ar}[H^+]}{\sum_{i=0}^{n} \prod_{r=0}^{i} K_{ar}[H^+]}, \quad (2)$$

where OD_{obs} is the observed optical density at a given wavelength, OD_0 is the optical density at the alkaline edge, DOD_i is the optical density change related to the ith pH-dependent optical transition, K_{ar} is the equilibrium constants for the rth protonation step, such that $K_{a0} \times [H^+] = 1$, and n is the total number of protonating groups.

The pH dependence of the kinetics for CO binding to Fe(II) forms of both hemes is described according to the following equation:

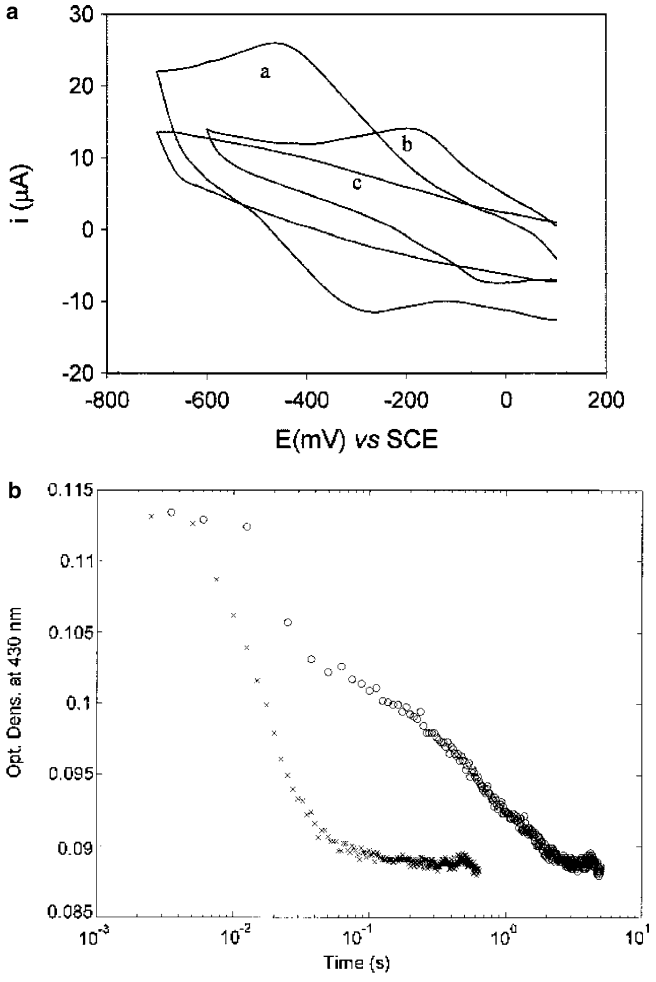

Fig. 1 **a** Cyclic voltammograms of protohemin-6(7)-*l*-histidine methyl ester (*heme-H*) at pH 7.0 in 30% dimethyl sulfoxide (*DMSO*) (*a*), in 100% DMSO (*b*) and in 20 mM phosphate pH 7.0 without DMSO (*c*). Sweep rate 100 mV/s, 20 °C. **b** Progress curves of CO binding to heme-H in the absence of DMSO (*circles*) and in the presence of 30% DMSO (*crosses*) at pH 5.5. CO concentration 0.5 mM after mixing, 20 °C. For further details, see text

$$l'_{\mathrm{obs}} = \sum_{i=0}^{n} l'_i \frac{\prod_{r=0}^{i} K_{\mathrm{ar}}[H^+]}{\sum_{i=0}^{n}\prod_{r=0}^{i} K_{\mathrm{ar}}[H^+]}, \qquad (3)$$

where l'_{obs} is the observed second-order rate constant for CO binding, l'_i (with $i = 0, \ldots, n$) are the rate constants of the ith-protonated species and K_{ar} are the binding constants for the rth proton, such that $K_{\mathrm{a}} = 10^{\mathrm{p}K_{\mathrm{a}}}$, with $K_{\mathrm{a0}} \times [\mathrm{H}^+] = 1$.

Global fitting was carried out as described elsewhere [30], by combining the parameters obtained through the fitting of the pH dependence of redox potentials (Eq. 1), absorption spectra (Eq. 2) and CO binding kinetics (Eq. 3). All these data were merged and a least-squares fitting procedure of the overall data set was carried out, employing for each set of data the corresponding equation, but interconnecting the fitting outcome in order to find the minimum number of parameters (i.e., pK_{a} values) required for the global description of their pH dependence. Therefore, the overall description and the number of parameters is clearly redundant for each separate set of data (i.e., redox potentials, absorption spectra and CO binding kinetics), but it is the minimal number of protonation events for the whole system.

NMR experiments

The ^{1}H-NMR spectra of the cyanide adducts of heme-H and heme-GH, obtained by addition of a small excess of KCN in deuterated methanol, were recorded with a Bruker AVANCE 400 spectrometer, operating at a proton frequency of 400.13 MHz. For the preparation of the reduced heme, ferric heme-GH was dissolved in degassed deuterated DMSO containing 5% (v/v) of 200 mM aqueous phosphate buffer and reduced by addition of a small excess of dithionite under anaerobic conditions in a gas-tight NMR tube.

Results

Characteristics of the chelated protoheme derivatives

Chelated heme derivatives obtained by covalent attachment of the axial donor residue to one of the propionic acid side chains of natural porphyrins consisted of an equimolar mixture of the two isomers carrying the substituent in position 6 or 7 of the porphyrin ring, which could not be separated by thin-layer chromatography or HPLC. The isomer composition is clearly shown by the NMR spectrum of the ferric cyanide derivative of the heme complex, which exhibits sufficiently narrow paramagnetic signals (see for instance the spectrum of heme–GH–CN$^-$ in the supplementary material) [28, 31, 32]. Coordination of the donor substituent to an axial position of the iron center can occur above or below the porphyrin plane, thus producing a total of four diastereoisomeric chelated heme derivatives. The observation of only two isomers in the NMR spectra indicates that the exchange of the donor group on the side chain between the two axial positions of each isomer is fast on the NMR time scale. The isomeric composition of the heme-H and heme-GH complexes is not expected to influence the spectral or redox properties of the heme chromophore; these properties strictly depend on the nature of the donor groups and on the coordination state of the metal ion, therefore they should be similar for the various isomers under investigation. On the other hand, the presence of multiple isomeric forms in solution has a strong influence on the circular dichroism (CD) spectra of the hemin complexes, resulting in an overlap of the contributions of the individual isomers, which likely brings about an extensive cancellation of CD activity. Therefore, the CD spectra of the present hemin complexes display very weak signals (data not shown).

Redox properties

Figure 2 shows the pH dependence of redox potentials vs. the normal hydrogen electrode for heme-H and heme-GH. Over the pH range investigated, both heme complexes display redox potentials ranging between −0.15 and +0.15 V. Such values are similar to those shown by a number of heme proteins, such as some peroxidases [33]; however, they are more positive than those of hemin [34–36], the two heme-containing fragments of horse cytochrome *c* (microperoxidase-8 [37, 38], microperoxidase-11 [39]) and horseradish peroxidase [40]. Furthermore, the redox potentials of heme-H and heme-GH are significantly lower than those of horse cytochrome *c* [41], owing to the nature of one residue (Met80) axially ligated to the heme iron in the protein. The methionine is in fact bound to the metal by a sulfur atom, a good electron acceptor, that favors the reduced state and increases the redox potential of the protein.

For both heme-H and heme-GH the redox properties appear to be modulated by the redox-linked protonation of (at least) two groups displaying different pK_a values, as reported in Table 1. While the group(s) with higher pK_a values is(are) similar for the two heme complexes, the group(s) displaying lower pK_a value(s) differ(s) by approximately two pH units (Table 1), reflecting structural differences between the two hemes. In this respect, it is noteworthy that the iron–histidine axial bond is more strained in heme-H than in heme-GH, as shown by thorough molecular mechanics and molecular dynamics calculations performed on the deuterohemin analogues of these complexes [18], owing to the different length of the arm connecting the propionate to the heme iron. This feature probably brings about a different bond energy for the axial coordination, thus affecting the pK_a value for the protonation of the N_ε of the imidazole group, which is the event most likely responsible for the $^{ox}pK_{a2}$ and $^{red}pK_{a2}$ of both hemes. However, the system may be more complex than it appears from this phenomenological analysis (see the dashed line in Fig. 2, corresponding to data in Table 1 for $n=2$), and it probably requires the presence of a third redox-linked group (see the continuous line in Fig. 2, corresponding to data in Table 1 for $n=3$). This possibility, which is confirmed by other methods (see later), involves a third redox-linked group with a lower pK_a value (Table 1), which indeed displays features expected for the protonation of the N_ε of the imidazole group (i.e., $^{ox}pK_{a3} > {}^{red}pK_{a3}$; Table 1), as observed in other heme model systems [42].

Furthermore, in pure DMSO the two hemes display fairly positive redox potentials (Fig. 2), very similar to those observed at acidic pH (approximately 3.5) in aqueous solutions. This behavior clearly indicates that in pure DMSO the protonating groups of the two hemes retain most of their protons, which are then released to the bulk solution upon water addition at weakly acidic and alkaline pH values; the consequent destabilization of the Fe(II) species leads to the less positive (or even negative) redox potentials observed in aqueous solution.

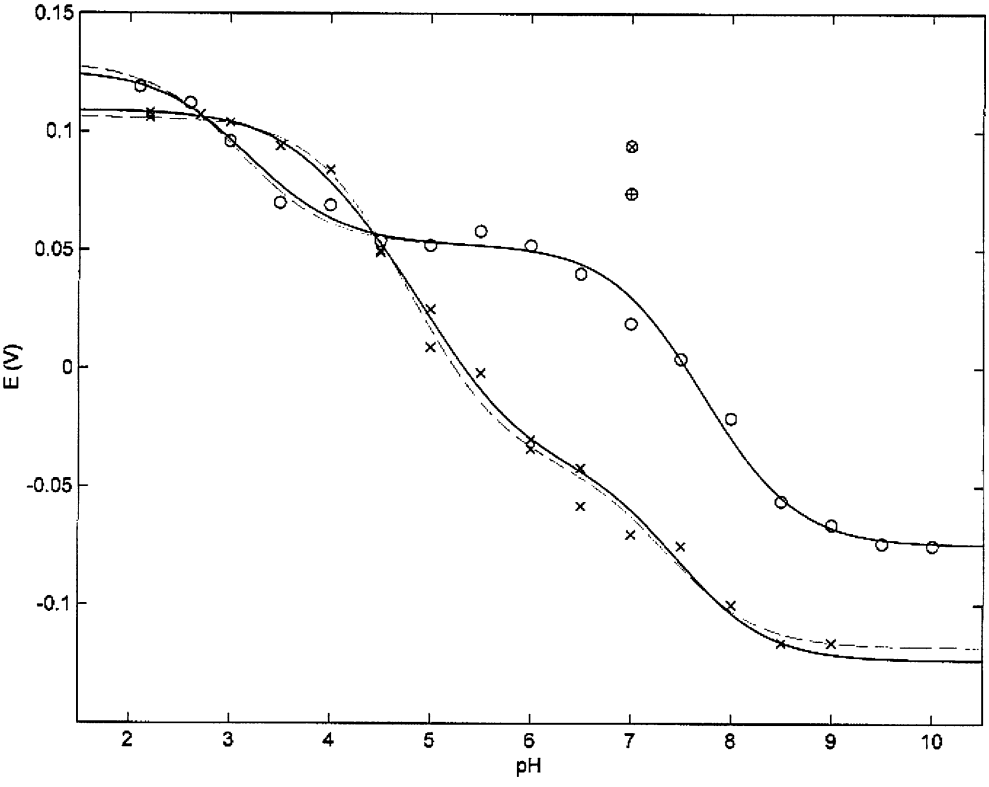

Fig. 2 pH dependence of redox potentials for heme-H (*crosses*) and protohemin-6(7)-glycyl-l-histidine methyl ester (*heme-GH*) (*circles*). *Dashed lines* are the nonlinear least-squares fitting of the data according to Eq. 1, employing $n=2$ (see Table 1); *continuous lines* are the nonlinear least-squares fitting of the data according to Eq. 1, employing $n=3$ (see Table 1). In both cases $E_0=-0.118$ V for heme-H and $E_0=-0.075$ V for heme GH (see Eq. 1). Symbols ⊗ and ⊕ refer to redox potentials in pure DMSO for heme-H and heme-GH, respectively. For further details, see text

Spectroscopic properties

In order to better understand the relationship linking the structural and redox properties of the two heme complexes, the spectroscopic features of their ferrous forms were investigated as a function of pH. Figures 3a and 4a show the Soret absorption spectra as a function of pH for heme-H and heme-GH, respectively. The proton-linked behavior of both heme complexes appears to be complex, displaying multiple proton-linked transitions. In particular, the λ_{max} of the heme-H absorption spectrum, centered at 423 nm at alkaline pH, shifts to 417 nm as the pH is lowered (Fig. 3a). The pH-dependent transition (obtained from the absorption values at 417 and at 423 nm) is shown in Fig. 3b. The proton-linked spectral changes for heme-GH, shown in Fig. 4, are more complex. As shown in Fig. 4a, the pH-dependent spectroscopic properties of heme-H and heme-GH look similar down to pH 5; however, a new species (not observed for heme-H) appears at lower pH, being characterized by a further blueshift and a weakening of the Soret band. Such a different behavior is clearly observable in Figs. 3b and 4b; while at 423 nm the optical absorption spectrum of heme-GH shows a pattern similar to that of heme-H, at 417 nm the trend is significantly distinct, displaying an absorbance decrease at pH < 4.0. Spectroscopic data in the visible range suggest that both hemes are six-coordinated over the whole pH range investigated (Figs. 3c, 4c); in the intermediate pH range, a water and/or a DMSO molecule are/is likely bound *trans* to the axial imidazole, while two of these molecules seem to be bound to iron(II) at acidic pH.

Both heme-H and heme-GH display similar pK_a values for the spectral variations, even though at different wavelengths a different contribution from the various protonating groups is detected (Table 2). In particular, for both hemes the value of $^{sp}pK_{a1}$ for the optical transitions is very similar to the $^{red}pK_{a1}$ value from the redox measurements (Table 1 for $n = 2$ and for $n = 3$), suggesting that the protonating group, which modulates redox equilibria, also plays an important role in the events regulating the optical changes detected for the reduced hemes.

Besides this group, fitting of spectroscopic data suggests that two additional groups are important, one of which, identified as $^{sp}pK_{a2}$, displays very similar pK_a values for heme-H and heme-GH (i.e., 5.31 ± 0.16 and 5.19 ± 0.15, respectively; Table 2). The protonation of this group upon a pH jump from pH 7.0 to pH < 5.0 appears to be associated with a spectroscopic transition, which is very fast for heme-H (data not shown), taking place within the dead time of the stopped flow, while it is slower for heme-GH, being completed in approximately 0.1 s, so in this case the process can be followed both in the Soret region (Fig. 5a) and in the visible range (Fig. 5b). This clearly demonstrates that the spectroscopic change of the Fe(II) heme observed in the Soret region reflects a transition between two six-coordinated species.

The third group responsible for the pH dependence of the spectroscopic properties, identified as $^{sp}pK_{a3}$ (Table 2), displays drastically different values between heme-H and heme-GH, as for $^{red}pK_{a2}$ (Table 1 for $n = 2$), but with values much more similar to those of $^{red}pK_{a3}$ (Table 1 for $n = 3$ and Table 2), giving strength to the idea of the existence of a third redox-linked protonating group (see before), which is better observed by absorption spectroscopy.

The NMR spectra of ferrous heme-GH in DMSO containing a small amount of buffer at pH 7.0 or 2.4 indicate the presence of low-spin, diamagnetic species with all signals falling in the 0–10-ppm range (see supplementary material). Unfortunately, the spectra are complicated by the presence of isomers, and it is therefore difficult to make a complete assignment of the signals. However, the marked differences observed in the 0.5–4.5- and 5.5–8.5-ppm ranges can be attributed, with the help of two-dimensional NMR experiments, to structural changes induced in both the amino acid and propionic acid arms by the pH change.

Table 1 Values of pK_a for oxidized and reduced forms of protohemin-6(7)-L-histidine methyl ester (*heme-H*) and protohemin-6(7)-glycyl-L-histidine methyl ester (*heme-GH*) from direct current cyclic voltammetry at 20 °C

	Heme-H	Heme-GH
$n = 2$		
$^{ox}pK_{a1}$	7.08 ± 0.18	7.25 ± 0.15
$^{ox}pK_{a2}$	4.24 ± 0.17	2.82 ± 0.16
$^{red}pK_{a1}$	7.66 ± 0.15	8.19 ± 0.17
$^{red}pK_{a2}$	5.31 ± 0.16	3.38 ± 0.17
$n = 3$		
$^{ox}pK_{a1}$	7.16 ± 0.16	7.25 ± 0.16
$^{ox}pK_{a2}$	4.01 ± 0.18	3.82 ± 0.17
$^{ox}pK_{a3}$	4.45 ± 0.16	2.89 ± 0.17
$^{red}pK_{a1}$	7.78 ± 0.17	8.19 ± 0.15
$^{red}pK_{a2}$	5.31 ± 0.18	3.38 ± 0.17
$^{red}pK_{a3}$	4.24 ± 0.17	3.87 ± 0.16

CO binding properties

Figure 6 reports the time-dependent spectral changes at pH 7.0 induced by the reaction of heme-H (Fig. 6a) and heme-GH (Fig. 6b) with 20 μM CO. In both cases, the reaction is characterized by clear isosbestic points, consistent with the existence of only two species: the Fe(II) form (with a Soret $\lambda_{max} = 423$ nm) and the CO-bound form ($\lambda_{max} = 417$ nm and a higher extinction coefficient). Therefore, in this reaction a weakly bound solvent molecule is replaced by the much stronger ligand CO as the axial heme ligand. However, when the Fe(II) hemes are reacted with the same amount of CO after a pH jump from pH 7.0 to pH < 5 (i.e., pH values at which the second group, characterized by $^{sp}pK_{a2}$, becomes protonated, see before) a much more complex

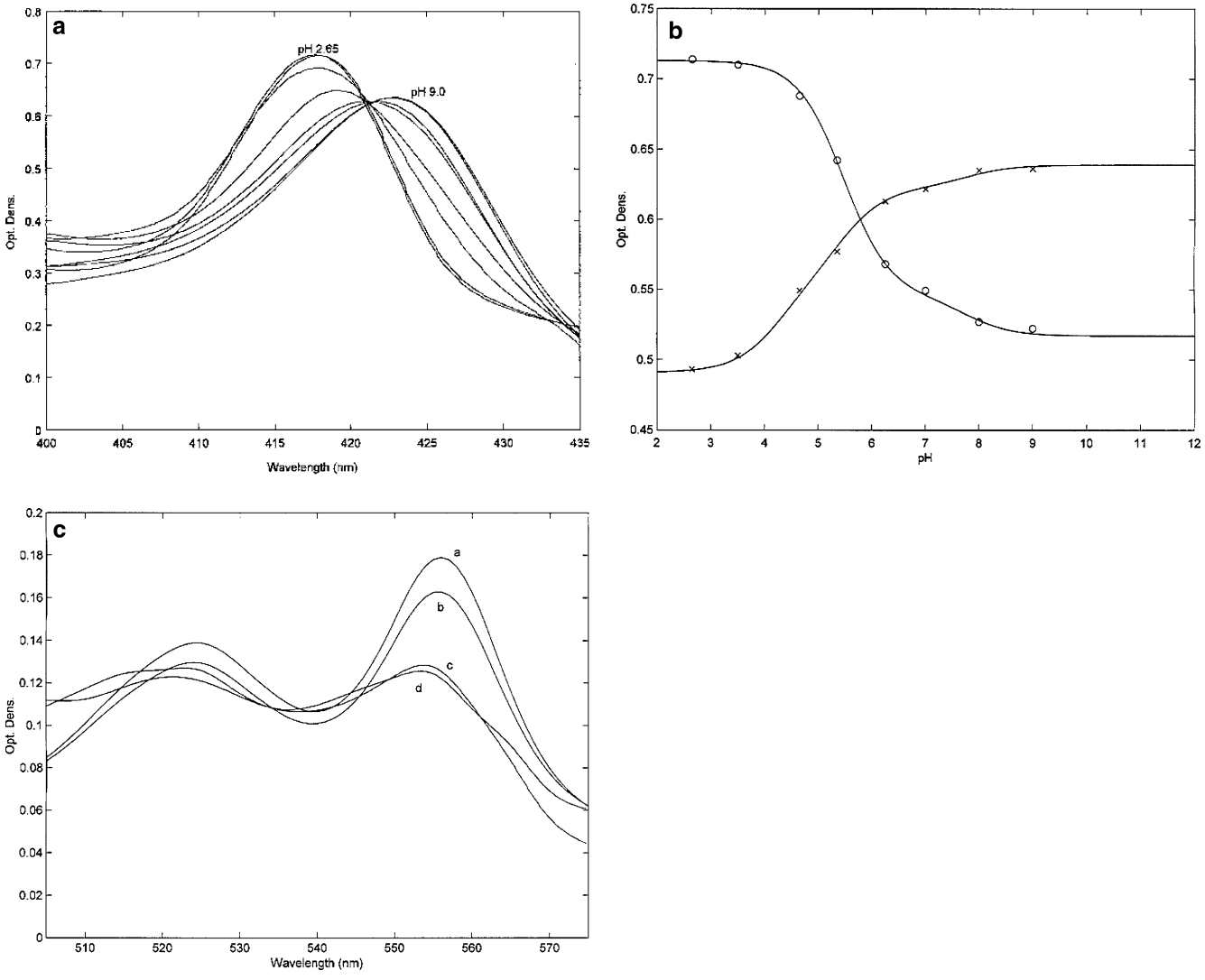

Fig. 3 pH dependence of optical spectra for the unliganded Fe(II) form of heme-H in the Soret region (**a**) and in the visible (**c**) range. Spectra at pH < 5 were obtained by mixing deoxygenated solutions of heme-H at pH 7.0 (in low ionic strength buffer) with a buffer of the desired pH, in the presence of sodium dithionite. The spectrum shown refers to the final stable species, attained within 1 ms (i.e., mixing dead time of the stopped flow). **b** pH dependence of the absorbance value, at $\lambda = 417$ nm (*circles*) and $\lambda = 423$ nm (*crosses*). The *lines* were obtained from Eq. 2 utilizing the $^{sp}pK_a$ values reported in Table 2. **c** Absorption spectra of the unliganded Fe(II) form of heme-H in the visible range at pH 9.0 (*a*), at pH 7.0 (*b*), at pH 4.2 (*c*) and at pH 2.4 (*d*). For further details, see text

kinetics behavior is observed. This is not unexpected, because the spectral changes associated with the pH change (from pH 7.0 to pH < 5.0) occur with different rates for heme-H and heme-GH. For heme-H the optical pH-dependent transition of the Fe(II) heme is very fast and occurs within the dead time of the instrument. Thus, in this case the observed reaction only refers to the CO binding process to the protonated species with a clear isosbestic point. As shown in Fig. 6c at pH 2.4, the absorbance peak of the Fe(II) heme-H centered at 417 nm shifts along the reaction with CO toward the blue to give a complex characterized by a Soret peak at 411 nm and a decreased extinction coefficient.

On the other hand, for heme-GH the pH-dependent optical transition of the Fe(II) heme (Fig. 5a) falls in the observation time range and partially interferes with the CO binding kinetics, thus bringing about a more complex spectroscopic time evolution (Fig. 6d). As a matter of fact, for heme-GH at pH 2.4 the first observed species, characterized by $\lambda_{max} = 423$ nm, rapidly evolves toward a species characterized by $\lambda_{max} = 417$ nm and a higher extinction coefficient (as previously reported; Fig. 5a), which further proceeds to a CO-bound form (Fig. 6d) very similar to that observed for heme-H at the same pH (Fig. 6c). Such spectroscopic features, revealed by the progress curves at different wavelengths (Fig. 6e), which refer to CO binding to the two hemes at pH 2.4, clearly indicate that for both hemes the CO-bound form at pH 7.0 (Fig. 6a, b) is different from the CO-bound form at acid pH values (Fig. 6c, d). In the visible range the CO-bound spectra of the two hemes do not show any

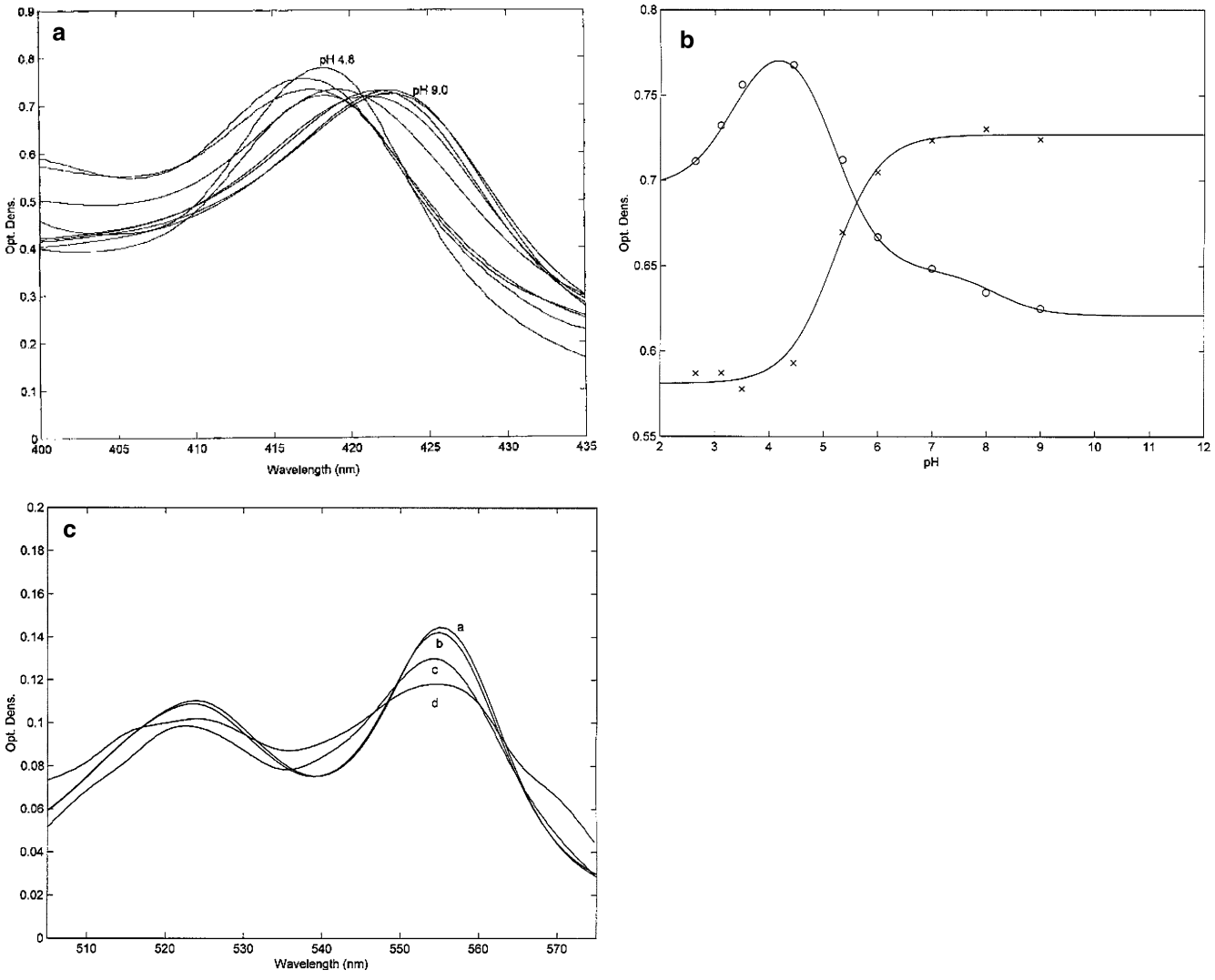

Fig. 4 pH dependence of the absorption spectra of the unliganded Fe(II) form of heme-GH in the Soret region (**a**) and in the visible range (**c**). **b** pH dependence of the absorbance value at $\lambda = 417$ nm (*circles*) and $\lambda = 423$ nm (*crosses*). The *lines* were obtained as described in the legend to Fig. 2. **c** Absorption spectra of the unliganded Fe(II) form of heme-GH in the visible range at pH 9.0 (*a*), at pH 7.0 (*b*), at pH 4.2 (*c*) and at pH 2.4 (*d*). **d** Absorption spectra of the Fe(II) "unligated" species for heme-GH in 30% DMSO (*a*) and in pure DMSO (*b*); in the visible region absorption spectra have been magnified 5 times. For further details, see text

appreciable pH dependence (data not shown), thus confirming that they remain six-coordinated; however, a different nature for the axial ligands at neutral pH cannot be ruled out.

In contrast to the fairly large changes observed in the absorption spectra, CD spectra recorded as a function of pH are less informative, being essentially flat in the Soret region (data not shown). The very weak optical activity exhibited by heme-H and heme-GH depends only in part on the fact that the two complexes are a mixture of isomers, because the corresponding ferric forms exhibit very weak but observable CD spectra (data not shown). The weaker binding strength of the axial imidazole group to Fe(II), as well as the larger kinetic lability of

Table 2 Values of pK_a for the description of absorption optical transitions in heme-H and heme-GH at different wavelengths

	Heme-H	Heme-GH
417 nm		
$^{sp}pK_{a1}$	7.78 ± 0.14	8.19 ± 0.14
$^{sp}pK_{a2}$	5.31 ± 0.16	5.19 ± 0.15
$^{sp}pK_{a3}$	–	3.38 ± 0.16
423 nm		
$^{sp}pK_{a1}$	7.78 ± 0.15	–
$^{sp}pK_{a2}$	5.31 ± 0.15	5.19 ± 0.15
$^{sp}pK_{a3}$	4.24 ± 0.14	–
555 nm		
$^{sp}pK_{a1}$	7.78 ± 0.16	8.19 ± 0.14
$^{sp}pK_{a2}$	5.31 ± 0.17	5.19 ± 0.15

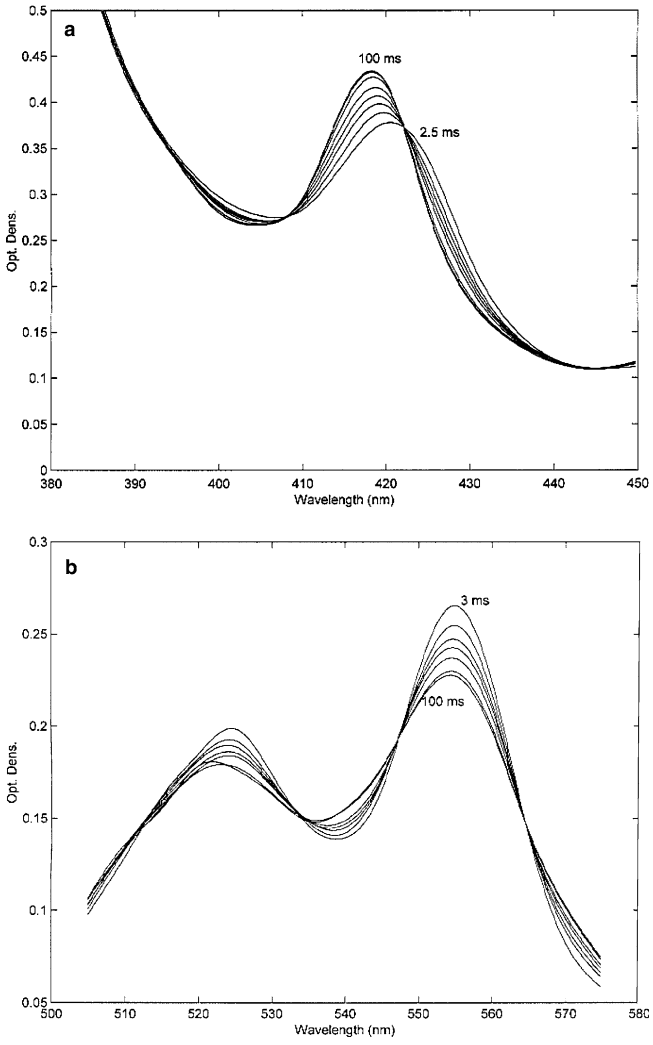

Fig. 5 Transient spectra of the unliganded Fe(II) form of the heme-GH in the Soret region (**a**) and in the visible range (**b**) obtained after mixing the heme with buffer to a final pH of 4.2; this behavior is observed also at lower pH values. For further details, see text

Fe(II) with respect to Fe(III) bonding, likely results in a faster exchange of the side arm carrying the axial donor between the two positions above and below the porphyrin plane, resulting in an epimerization process for the reduced complexes. Support of this view comes from the observation that the CD spectra of the Fe(II)–CO forms, where the metal centers carry a strong and *trans*-stabilizing axial ligand, are appreciably more intense (see later) (Fig. 7). At pH 7.0, the CO-bound forms of both heme complexes exhibit very similar CD spectra, featuring a weak negative peak at 418 nm nearly coincident with the absorption maximum (417 nm). This indicates that the dominant isomer of the Fe(II)–CO complexes has the same chirality for both heme-H and heme-GH derivatives. The Soret CD curves of the Fe(II)–CO complexes become two-signed at pH 4.8, with magnified optical activity, but curiously the pattern observed for heme-H (negative peak at 412 nm, positive peak at 432 nm; Fig. 7a) is the mirror image of that exhibited by heme-GH (positive peak at 405 nm, negative peak at 430 nm; Fig. 7b). A two-signed CD behavior in the Soret region is frequently observed for Fe(II)–CO complexes of heme proteins [43–45] and only reflects the fact that the Soret band encompasses two nearly degenerate transitions [46]. In the present case, the opposite CD pattern displayed by the Fe(II)–CO complexes of heme-H and heme-GH is probably due to the fact that the isomer with dominant CD activity is different in the two cases.

By following the absorption spectroscopic variations we have sorted out the CO binding kinetics at several different pH values and the resulting bimolecular rate constants are reported for both hemes in Fig. 8 as a function of pH. It is evident that above pH 7.0 both hemes display the slowest reacting form (with heme-H slightly faster than heme-GH). At pH below 7.0 the bimolecular rate constant progressively increases, clearly indicating that the group responsible for $^{red}pK_{a1}$ (from the pH dependence of the redox properties; Table 1) and for $^{sp}pK_{a1}$ (from the pH dependence of the spectroscopic properties; Table 2) does not affect the CO binding kinetics. The lines represent the best fitting according to Eq. 3 with $n = 3$ (Table 3), underlying that the CO binding process is modulated by the protonation of three groups in addition to $^{red}pK_{a1}$.

It is very important to note that for both hemes $^{kin}pK_{a1}$ and $^{kin}pK_{a2}$ (Table 3) correspond to $^{sp}pK_{a2}$ and $^{sp}pK_{a3}$, respectively (Table 2), which indicates that the two groups involved are simultaneously affecting to some extent the CO binding kinetics and conformational transitions corresponding to the spectroscopic variations. In addition, the groups responsible for $^{kin}pK_{a2}$ and $^{kin}pK_{a3}$ (Table 3) display fairly low pK_a values in both hemes, with $^{kin}pK_{a2}$ associated with an enhancement of the CO binding rate constant and $^{kin}pK_{a3}$ slightly decreasing the rate constant. In addition, for heme-GH both groups display pK_a values very similar to $^{red}pK_{a2}$ (Table 1), which might suggest their involvement in the modulation of redox properties. Therefore, we carried out a further analysis of the pH dependence of redox properties of both heme-H and heme-GH, employing three ($n = 3$, Table 1) redox-linked groups, by imposing three of the four pK_a values resulting from the combined analysis of redox, spectroscopic and CO binding kinetics analysis of the pH dependence (Tables 1, 2, 3). This analysis (see the continuous lines in Fig. 2) gives very satisfactory results (since the occurrence of three redox-linked groups allows us to describe the pH dependence of redox properties with $^{red}pK_a$ values), perfectly compatible with those resulting from the pH dependence of spectroscopic and CO binding kinetics properties. At the same time, the values of $^{ox}pK_a$ and $^{red}pK_a$ obtained for the protonation of the Fe–N_ε bond are compatible with those observed in all other systems. Therefore, at this stage it is possible to describe the overall pH-dependent behavior of the two hemes by four protonating groups, three of which are redox-linked. Each heme shows one residue, not required for the pH dependence of redox

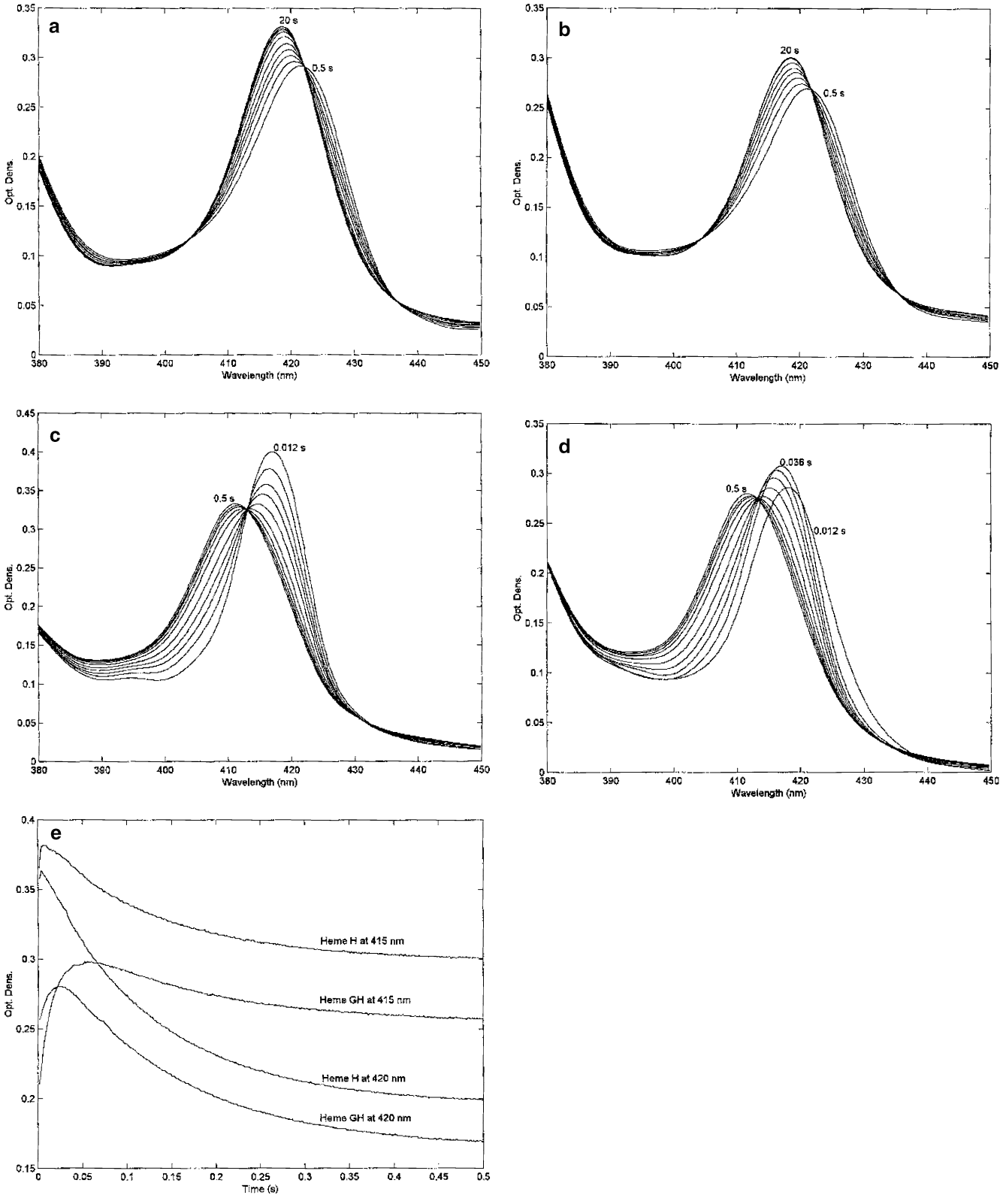

Fig. 6 Transient spectroscopic changes obtained after mixing heme-H at pH 7.0 (**a**) and at pH 2.4 (**c**), and heme-GH at pH 7.0 (**b**) and at pH 2.4 (**d**) with 20 μM CO (final concentration after mixing). Unliganded Fe(II) hemes at pH 7.0 in very low ionic strength buffer were mixed with the high ionic strength buffer ($I = 0.1$ after mixing) at the desired pH and CO concentration. **e** Kinetics progress curves at 415 and 420 nm (as indicated), following the mixing of heme-H and/or heme-GH (as indicated) with 20 μM CO final concentration at pH 2.4. For further details, see text

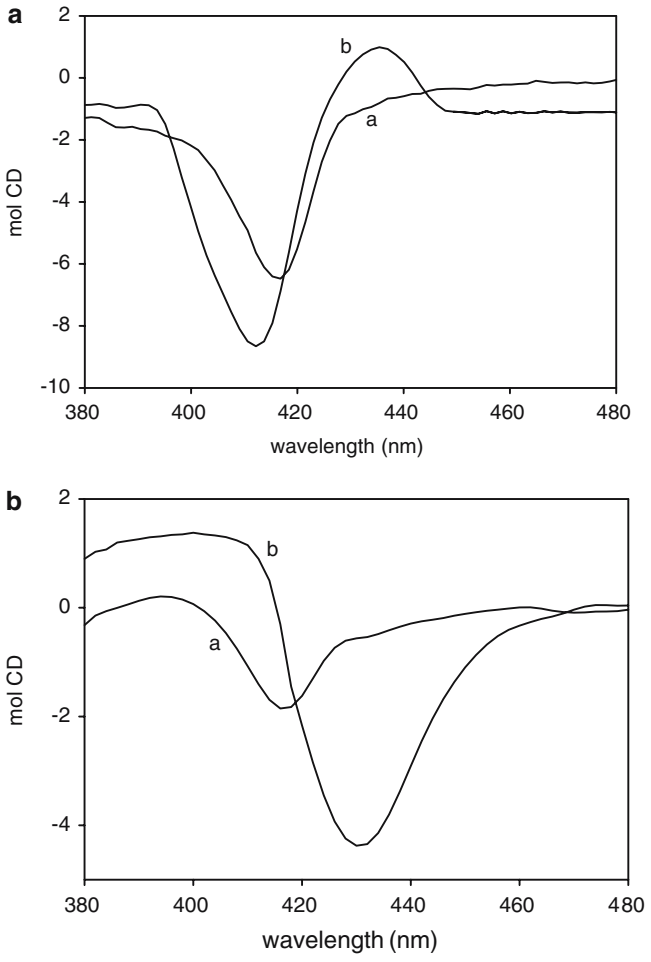

Fig. 7 Circular dichroism spectra of Fe(II) CO-bound species of heme-H (**a**) and heme-GH (**b**) at pH 7.0 (*a*) and at pH 4.8 (*b*). For further details, see text

properties (thus not redox-linked), but playing a role for the modulation of spectroscopic properties and CO binding kinetics; in such a case the pK_a value of the Fe(III) species has been considered arbitrarily the same as for the Fe(II) form. The overall sketch is reported in Schemes 2 and 3, where the complex proton-, redox- and ligand-linked modulations of the structural and functional properties of these two hemes are quantitatively described with all values of ^{III}pK_a (for the oxidized form) and of ^{II}pK_a (for the reduced form), redox potentials and kinetics rate constant for the four protonation steps, as resulting from this global analysis, independently of the method employed for their determination.

Discussion

The finding that the overall proton-linked modulation of redox, spectroscopic and CO binding kinetics properties can be described for heme-H and heme-GH complexes by the shift of pK_a values of four groups may be in keeping with the consideration that indeed, over the pH range between 2 and 10, there are four groups, which can in principle display changes of pK_a upon reduction and/or CO binding. These can be (1) coordinated H_2O, (2) one of the heme propionates, (3) the N_ε of the coordinating imidazole and (4) the carboxylate of the histidine residue upon hydrolysis of the methyl ester group (in acid medium).

In particular, ^{II}pK_{a1}, which seems important for the pH dependence of redox properties (Fig. 1, Table 1) and for the spectroscopic features of the two Fe(II) hemes (Figs. 3, 4, Table 2), does not appear to affect CO binding kinetics to an appreciable extent (Schemes 2, 3). Therefore, ^{II}pK_{a1} can be tentatively attributed to the deprotonation of the labile coordinated water. This assignment is not contradicted by the fact that the protonation equilibria of H_2O do not affect the CO binding rate constant, since it is known that even in deoxymyoglobin this water molecule is at approximately 3.0 Å from the iron [47] and it does not affect the ligand binding rate constant. It is also important to outline that the values of ^{III}pK_{a1} and ^{II}pK_{a1} (Schemes 2, 3) are similar for the two heme complexes; therefore, the redox-linked behavior of the Fe–H_2O complex is only marginally affected by the length of the coordinating arm (and thus by the strain exerted at the level of the axially coordinating arm).

On the other hand, the group responsible for ^{II}pK_{a2} in Schemes 2 and 3 appears to be crucial for controlling the structural change responsible for the spectroscopic variations (Figs. 3, 4, Table 2); its protonation in the Fe(II) species brings about for both hemes an almost tenfold CO binding rate enhancement (Table 3, Fig. 8). Furthermore, this group turns out to be redox-linked in heme-H but not (or onyl very weakly) in heme-GH. The heme propionate can be tentatively identified as responsible for pK_{a2}; this group may have an important structural effect, since it can be involved in a network of hydrogen bonds with the axially bound water molecule. Upon protonation, the whole hydrogen-bonding network is broken and the binding of CO becomes easier, accounting for the marked effect of its protonation on the CO binding rate constant. Although pK_{a2} appears to be higher than expected for a propionate group, its value is likely affected by the solvent mixture containing DMSO. This suggests that the protonation of the H_2O molecule (associated with pK_{a1}) and the protonation of the propionate with the consequent alteration of the hydrogen-bonding network (associated with pK_{a2}) might facilitate the substitution of the H_2O molecule by DMSO, bringing about a spectral change (Figs. 3, 4, 5) similar to that observed in pure DMSO (Fig. 4d). Furthermore, since the associated spectral change is much faster in heme-H than in heme-GH (Fig. 5) it turns out that the relaxation rate corresponding to the proton-linked structural rearrangement of the hydrogen-bonding network is indeed affected by the strain exerted at the proximal level on the Fe–imidazole bond. In addition, this protonation brings about a marked enhancement of the

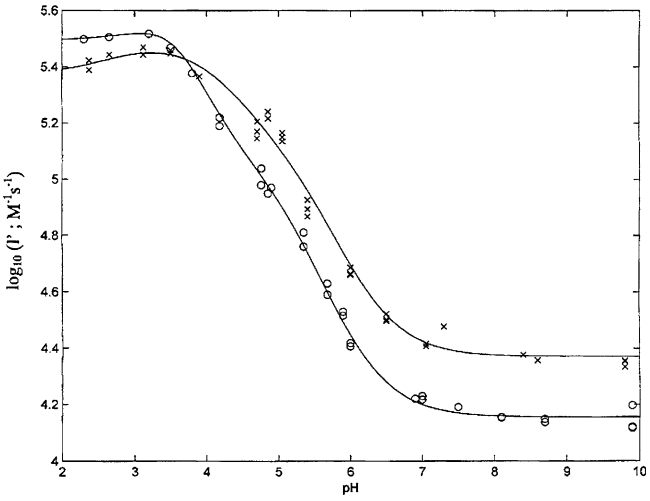

Fig. 8 pH dependence of the second-order kinetics constant for CO binding to heme-H (*crosses*) and heme-GH (*circles*). The *lines* were obtained by nonlinear least-squares fitting of data employing Eq. 3 with $n = 3$ and with the parameters reported in Table 3. For further details, see text

CO binding rate constant, clearly indicating that the hydrogen-bonding network of the coordinating H_2O represents a main determinant of the activation barrier for CO binding at pH > 6.0.

The different redox-linked behavior shown by heme-H and heme-GH for pK_{a2} may be related to the fact that protonation of the propionate occurs over the same pH range of the group associated with pK_{a3} in heme-H, whereas in heme-GH the two processes display pK_a values far apart (Schemes 2, 3), clearly suggesting that the two events are interconnected.

The behavior observed for the group responsible of the pK_{a3} value in Schemes 2 and 3 indicates that this group plays a relevant role in the modulation of the redox properties, the spectroscopic features (for heme-H) as well as the CO binding behavior of the heme group. In addition, the pK_{a3} value is drastically different between heme-H and heme-GH, suggesting that this group is indeed very sensitive to the structural differences between the two hemes. Indeed, the major difference between heme-GH and heme-H is the length of the coordinating arm, and thus the strain exerted on the axial bond between the heme iron and the N_ε of the imidazole; as a matter of fact, this different strain has already been proposed to account for the different properties of the corresponding deuterohemin derivatives [18]. Therefore, the weaker Fe–N_ε bond in heme-H is responsible for the higher pK_{a3} observed for this compound with respect to heme-GH (Schemes 2, 3). The observation that protonation of the propionate has a pK_a higher than that for the N_ε of the proximal imidazole is not surprising, in view of the fact that this nitrogen is involved in the bond with Fe(II), which dramatically lowers its pK_a [2, 3]. The value of ^{II}pK_{a3} in heme-GH (Table. 1, 3, Scheme 3) is very similar to that reported previously for the protonation of the N_ε of the proximal imidazole in myoglobin and hemoglobin [2, 3], in which a marked increase of CO binding was observed as well upon cleavage (or severe weakening) of this proximal bond. Protonation of the proximal imidazole group, and the consequent cleavage of the Fe–N_ε bond, induces a large effect on the redox properties, mainly for heme-H (Fig. 2, Scheme 2), and on the CO binding properties, mainly for heme-GH (Scheme 3), which become faster than for heme-H (Fig. 7). This feature is consistent with a bigger role played by the Fe–imidazole bond in shaping the activation barrier for CO binding to heme-GH with respect to heme-H. This is probably to be correlated with the higher energy of this bond in heme-GH due to the lesser strain. Furthermore, in the case of heme-H the cleavage of the Fe-imidazole bond occurs over the same pH range in which the propionate interacting with the hydrogen-bonding network of the axially coordinating H_2O undergoes protonation (Scheme 2). This partially hides the spectroscopic changes of heme-H, which indeed look simpler (Fig. 3). On the other hand, the much lower value of pK_{a3} in heme-GH (Scheme 3) renders this event spectroscopically more evident (Fig. 4). In addition, the partial overlap of the pH range over which the events correlated to the protonation of groups responsible for pK_{a2} and pK_{a3} occur in heme-H may help to explain the different behavior displayed by the two hemes for these two groups. Thus, in heme-H protonation of the propionate in the Fe(II) form has a ^{II}pK_a very similar to that observed in heme-GH (underlying a similar structural situation for the hydrogen-bonding network with the axially bound water molecule for the two hemes; Schemes 2, 3). However, in the reduced heme-H, the Fe–N_ε bond is cleaved at a pH value, corresponding to ^{II}pK_{a3}, only slightly lower than the pK_a of the propionate protonation, and at a pH even higher in the oxidized form, corresponding to ^{III}pK_{a3} (Scheme 2); thus, it falls in the range of the propionate protonation. Cleavage of the Fe–N_ε bond has a strong effect on the hydrogen bonding of the *trans* axially bound H_2O molecule (and thus on the protonation features of the propionate); therefore, the different protonation properties shown by the two groups in the two oxidation states render the protonation of the propionate redox-linked in heme-H (Scheme 2). This inter-

Table 3 Kinetics parameters and pK_a values from the nonlinear least-squares fitting of CO binding kinetics to heme-H and heme-GH at 20 °C

	Heme-H	Heme-GH
l'_1 ($M^{-1}s^{-1}$)	$2.35(\pm0.29)\times10^4$	$1.43(\pm0.17)\times10^4$
l'_2 ($M^{-1}s^{-1}$)	$1.49(\pm0.17)\times10^5$	$1.16(\pm0.12)\times10^5$
l'_3 ($M^{-1}s^{-1}$)	$3.11(\pm0.35)\times10^5$	$5.48(\pm0.63)\times10^5$
l'_4 ($M^{-1}s^{-1}$)	$2.34(\pm0.31)\times10^5$	$3.11(\pm0.37)\times10^5$
^{kin}pK_{a1}	5.31 ± 0.15	5.19 ± 0.16
^{kin}pK_{a2}	4.24 ± 0.18	3.38 ± 0.17
^{kin}pK_{a3}	2.73 ± 0.16	3.83 ± 0.16

relationship does not take place in heme-GH because both $^{III}pK_{a3}$ and $^{II}pK_{a3}$ are much lower (Scheme 3); in this case, protonation of the propionate always occurs in the presence of an intact Fe–N_{ε} bond.

The group responsible for pK_{a4} plays in both hemes a role in the modulation of CO binding kinetics, being responsible for the rate decrease at very low pH values (Fig. 8); furthermore, in heme-GH it affects the spectroscopic properties at 417 nm and the redox properties (Schemes 2, 3). Although the acidic pH range is difficult to analyze with structural methods, preliminary data by mass spectroscopy give evidence of a rather rapid hydrolytic degradation of the amino acid tails of both heme-H and heme-GH, leading to a mixture of species (data not shown). On the basis of these data, we tentatively identify the group responsible for pK_{a4} as the carboxylate group resulting from hydrolysis of the histidine methyl ester residue at very acidic pH. This carboxylate group could easily hydrogen bond to the (protonated) N_{δ} of the axial imidazole, thereby strengthening the interaction of the proximal imidazole with the iron and affecting the rate of CO binding.

The correlation between the groups responsible for pK_{a3} and pK_{a4} may help in accounting for the different behavior observed in the two hemes for this group. Thus, in heme-H the carboxylate protonation occurs over a pH range at which both Fe(II) and Fe(III) species display a cleaved Fe–N_{ε} bond (the swinging arm is no longer coordinated to the heme); therefore, no redox-linked difference is expected for the protonation of the carboxylate under these conditions, as observed (Scheme 2). On the other hand, in reduced heme-GH the protonation of the carboxylate (corresponding to $^{II}pK_{a4}$; Scheme 3) occurs at a pH value at which the Fe–N_{ε} bond is still mostly intact (or slightly weakened); therefore, it is affected by the strain induced by the axial coordination, displaying a much higher value than that observed in heme-H. In the oxidized heme-GH, the

Scheme 2 Thermodynamic and kinetic relationships between different equilibria in heme-H

Heme-H

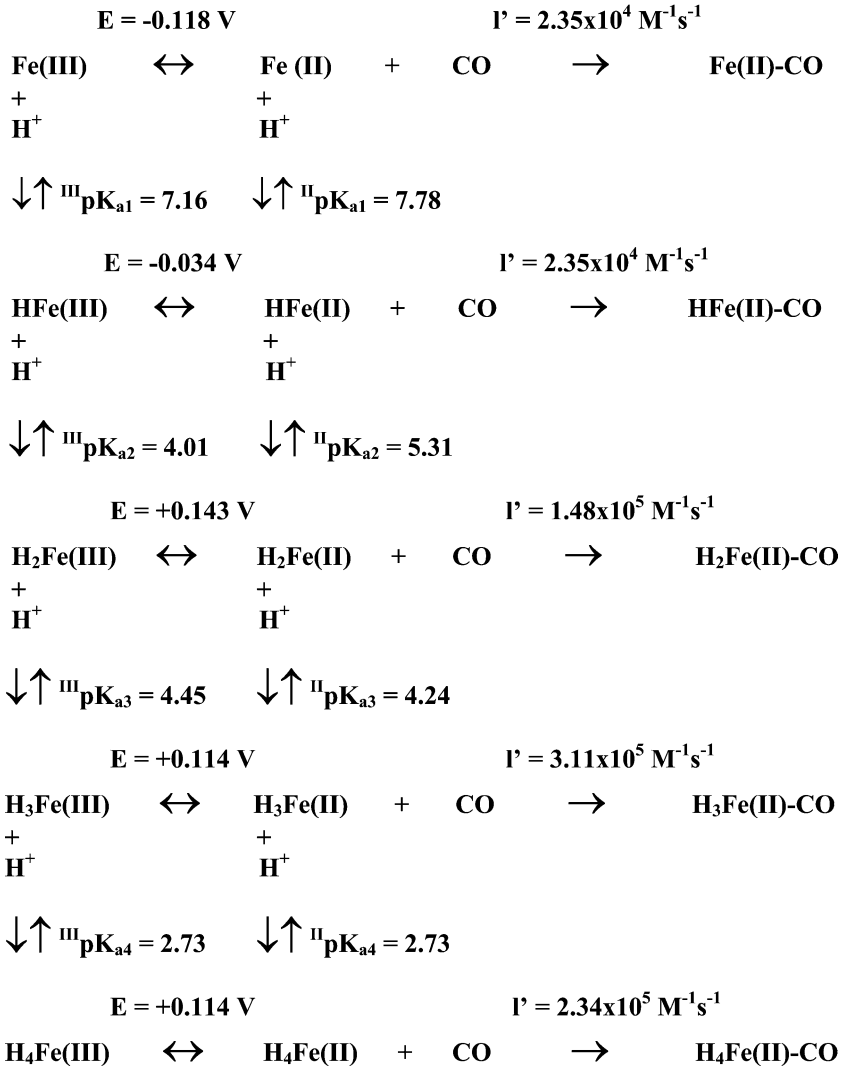

Scheme 3 Thermodynamic and kinetic relationships between different equilibria in heme-GH

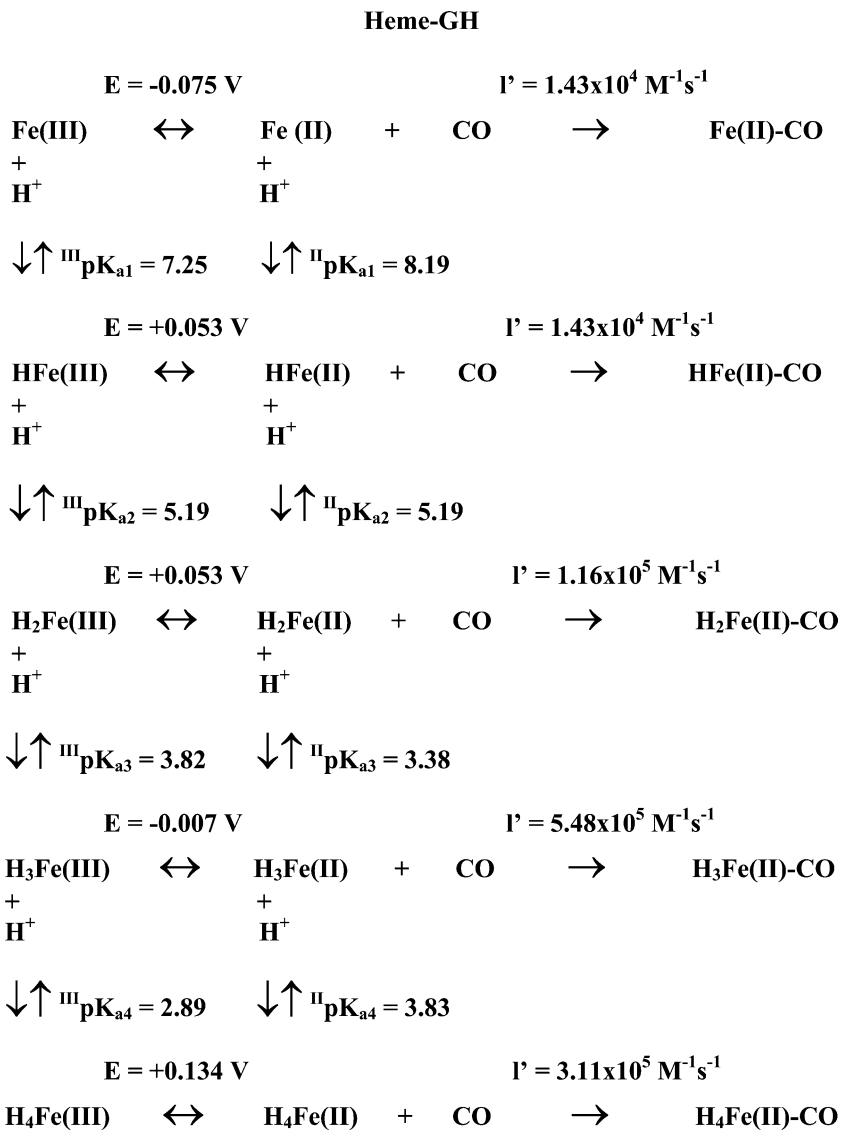

higher pH at which the Fe–N_ε bond is cleaved (see $^{III}pK_{a3}$ in Scheme 3) renders the situation much more similar to that observed in heme-H, bringing about a much lower pH for the protonation of the carboxylate group (see $^{III}pK_{a4}$ in Scheme 3).

At this stage, these attributions can only be considered as realistic ones; however, in the light of this hypothesis, we can try to account for the different behavior of the two hemes. As a whole, the picture emerging from this analysis points to a very relevant role played by the Fe–N_ε bond in these chelated heme complexes. It strongly affects the hydrogen-bonding network of the *trans* axially coordinated ligand (its cleavage dramatically alters the protonation properties of this network, see pK_{a2} for heme-H), underlying a communication between the two sides of the axial bonding of the heme. This interrelationship is not clearly observed in heme-GH simply because the protonation occurring in the hydrogen-bonding network of the axially coordinated H_2O takes place outside the range of the modification of the Fe–N_ε bonding in this heme. On the other hand, a close relationship between the Fe–N_ε coordination and the conformation of the coordinating arm is observed, such that the strain on it brings about a variation in the protonation properties of the carboxylate of the hydrolyzed histidine methyl ester. Such a feature can be correlated to the interrelationship in hemoproteins between the conformation of the axial coordination bond and the strain applied on the peptide associated with the coordinating residue. This phenomenon is observed in several hemoproteins, the most striking example being that of peroxidases, where a functional interrelationship has been documented between the proximal histidine and some residues on the proximal side of the heme pocket [48, 49]. Furthermore, a very relevant finding of this investigation is indeed represented by the unraveling of a continuum of energy communication between the two sides of the heme, such as the influence of the strain on the proximal side of the heme is transmitted to the protonation of the H_2O

molecule on the distal side of the heme (Schemes 2, 3), since it is demonstrated that the effect does not require the assistance of a protein matrix. Therefore, it seems evident that the modulation of the heme coordination and reactivity is only marginally altered by the protein matrix, whose main function appears to be that of shielding the active center from the bulk solvent rather than determining the reactive modes of the heme. The close similarity of the observed pK_a values with respect to those measured in hemoproteins [2, 3] strongly supports the view that in hemoproteins reactions occur at the heme almost independently of the protein matrix; however, the effect is then transmitted to the protein moiety, which undergoes conformational alteration(s). In this way, the protein moiety turns out to play a sort of wave-spread-out function, propagating the structural effects deriving from the reaction events occurring at the active site.

Acknowledgements This work was supported by COST D21 and MIUR (COFIN 2004055484). We thank G. Smulevich and A. Feis for several stimulating discussions.

References

1. Matsunaga I, Shiro Y (2004) Curr Opin Chem Biol 8:127–132
2. Coletta M, Ascenzi P, Traylor TG, Brunori M (1985) J Biol Chem 260:4151–4155
3. Coletta M, Ascenzi P, Brunori M (1988) J Biol Chem 263:18286–18289
4. Anzenbacher P, Dawson JH, Kitagawa T (1989) J Mol Struct 214:149–158
5. Shulman RG, Glarum SH, Karplus M (1971) J Mol Biol 57:93–115
6. Turner DL (1995) Eur J Biochem 227:829–837
7. Friedman JM (1985) Science 228:1273–1280
8. Momenteau M, Rougèe M, Loock B (1976) Eur J Biochem 71:63–76
9. Okuyama K, Murakami T, Nozawa T, Hatano M (1982) Chem Lett 111–114
10. Traylor TG, Lee WA, Stynes DV (1984) J Am Chem Soc 106:755–764
11. Traylor TG, Popovitz-Biro R (1988) J Am Chem Soc 110:239–247
12. Traylor TG, Ciccone JP (1989) J Am Chem Soc 111:8413–8420
13. Higuchi Y, Kusunoki M, Matsuura Y, Yasuoka N, Kakudo M (1984) J Mol Biol 172:109–139
14. Morgan B, Dolphin D (1987) Struct Bonding (Berlin) 64:115–204
15. Moura I, Teixeira M, Huynh BH, LeGall J, Moura JJG (1988) Eur J Biochem 176:365–369
16. Rivera M, Barillas-Mury C, Christensen KA, Little JW, Wells MA, Walker FA (1992) Biochemistry 31:12233–12240
17. Tsuchida E, Komatsu T, Arai K, Nishide H (1993) J Chem Soc Dalton Trans 2465–2469
18. Casella L, Monzani E, Fantucci P, Gullotti M, De Gioia L, Strini A, Chillemi F (1996) Inorg Chem 35:439–444
19. Monzani E, Linati L, Casella L, De Gioia L, Favretto M, Gullotti M, Chillemi F (1998) Inorg Chim Acta 273:339–345
20. Aron J, Baldwin DA, Marques HM, Pratt JM, Adams PA (1986) J Inorg Biochem 27:227–243
21. Munro OO, Marques HM (1996) Inorg Chem 35:3752–3767
22. Monzani E, Alzuet G, Casella L, Redaelli C, Bassani C, Sanangelantoni AM, Gullotti M, De Gioia L, Santagostini L, Chillemi F (2000) Biochemistry 39:9571–9582
23. Baldini S, Casella L, De Riso A, Monzani E, Profumo A, Roncone R (2003) In: Acosta M, Rodriguez-Lopez JN, Pedreño MA (eds) Plant peroxidases, biochemistry and physiology. University of Murcia, Spain, pp 62–67
24. Dallacosta C, Monzani E, Roncone R, Casella L (2003) In: Acosta M, Rodriguez-Lopez JN, Pedreño MA (eds) Plant peroxidases, biochemistry and physiology. University of Murcia, Spain, pp 97–103
25. Coletta M, Angeletti M, Ascone I, Boumis G, Congiu Castellano A, Dell'Ariccia M, Della Longa S, De Sanctis G, Priori AM, Santucci R, Feis A, Amiconi G (1999) Biophys J 76:1532–1536
26. Perutz MF (1972) Nature 237:495–499
27. Friedman JM, Rousseau DL, Ondrias MR, Stepnoski RA (1982) Science 218:1244–1246
28. Ryabova ES, Dikiy A, Hesslein AE, Bjerrum MJ, Ciurli S, Nordlander E (2004) J Biol Inorg Chem 9:385–395
29. Santucci R, Ferri T, Morpurgo L, Savini I, Avigliano L (1998) Biochem J 332:611–615
30. Ciaccio C, De Sanctis G, Marini S, Sinibaldi F, Santucci R, Arcovito A, Bellelli A, Ghibaudi E, Ferrari RP, Coletta M (2004) Biophys J 86:448–454
31. Casella L, Gullotti M, De Gioia L, Bartesaghi R, Chillemi F (1993) J Chem Soc Dalton Trans 233–2239
32. Casella L, Monzani E, Gullotti M, Gliubich F, De Gioia L (1994) J Chem Soc Dalton Trans 3203–3210
33. Santucci R, Bongiovanni C, Marini S, Del Conte R, Tien M, Banci L, Coletta M (2000) Biochem J 349:85–90
34. Clark WM (1972) Oxidation-reduction potentials of organic systems. Krieger, Huntington
35. Bianco P, Haladjian J, Draoui K (1990) J Electroanal Chem 279:305–314
36. Faraoni A, Santucci R, Campanella L, Tranchida G, Brunori M (1990) Biol Metals 3:122–124
37. Adams PA, Baldwin DA, Marques HM (1996) In: Scott RA, Mauk AG (eds) Cytochrome *c*. A multidisciplinary approach. University Science Books, Sausalito, pp 635–692
38. Marques HM (1990) Inorg Chem 29:1597–1599
39. Zamponi S, Santucci R, Brunori M, Marassi R (1990) Biochim Biophys Acta 1034:294–297
40. Ferri T, Poscia A, Santucci R (1998) Bioelectrochem Bioenerg 44:177–181
41. Moore GR, Pettigrew GW (1990) Cytochromes *c*. Evolutionary, structural and physiological aspects. Springer, Berlin Heidelberg New York
42. Safo MK, Nesset MJM, Walker FA, Debrunner PG, Scheidt WR (1997) J Am Chem Soc 119:9438–9448
43. Myer YP, Pande A (1978) In: Dolphin D (ed) The porphyrins, vol III. Academic, New York, pp 271–322
44. Casella L, Gullotti M, Pintar A, Marchesini A (1986) Biochim Biophys Acta 872:216–225
45. Sono M, Dawson JH, Ikeda-Saito M (1986) Biochim Biophys Acta 873:62–72
46. Hsu MC, Woody RW (1971) J Am Chem Soc 93:3515–3525
47. Yang F, Phillips GN Jr (1996) J Mol Biol 256:762–774
48. Smulevich G (1998) Biospectroscpy 4(Suppl 5):S3–S17
49. Ciaccio C, Rosati A, De Sanctis G, Sinibaldi F, Marini S, Santucci R, Ascenzi P, Welinder KG, Coletta M (2003) J Biol Chem 278:18730–18737